CHAPTER

Maps and sensorimotor transformations for eye-head gaze shifts: Role of the midbrain superior colliculus

2

A. John van Opstal*, Bahadir Kasap
Department of Biophysics, Donders Institute for Brain, Cognition and Behaviour, Radboud University Nijmegen, Nijmegen, The Netherlands
**Corresponding author: e-mail address: j.vanopstal@donders.ru.nl*

Abstract

Single-unit recordings in head-restrained monkeys indicated that the population of saccade-related cells in the midbrain Superior Colliculus (SC) encodes the kinematics of desired straight saccade trajectories by the cumulative number of spikes. In addition, the nonlinear main sequence of saccades (their amplitude–peak velocity saturation) emerges from a spatial gradient of peak-firing rates of collicular neurons, rather than from neural saturation at brain-stem burst generators. We here extend this idea to eye-head gaze shifts and illustrate how the cumulative spike-count in head-unrestrained monkeys relates to the desired gaze trajectory and its kinematics. We argue that the output of the motor SC is an abstract desired gaze-motor signal, which drives in a feedforward way the instantaneous kinematics of ongoing gaze shifts, including the strong influence of initial eye position on gaze kinematics. We propose that the neural population acts as a vectorial gaze pulse-generator for eye-head saccades, which is subsequently decomposed into signals that drive both motor systems in appropriate craniocentric reference frames within a dynamic gaze-velocity feedback loop.

Keywords

Motor map, Neural code, Kinematics, Eye-head coupling, Reference frames, Nonlinear pulse generator, Initial eye position

Progress in Brain Research, Volume 249, ISSN 0079-6123, https://doi.org/10.1016/bs.pbr.2019.01.006

1 Introduction

1.1 Eye-head gaze shifts

A saccadic eye-head gaze shift (ΔG) is the directional change of the fovea in space, which is determined by the sum of the changes of the eye-in-head and the head-on-neck orientations: $\Delta G = \Delta E + \Delta H$. The gaze-control system of human and non-human primates is optimally suited to reorient the fovea as fast and as accurately as possible to a target and to allow vision to identify objects with high resolution during intermittent fixations.

Although any particular gaze shift can in principle be generated by infinitely many combinations of eye and head contributions, under controlled initial conditions the system selects highly reproducible movement strategies. It has therefore been hypothesized (Goossens and Van Opstal, 2012; Harris and Wolpert, 1998, 2006; Kardamakis and Moschovakis, 2009; Sağlam et al., 2011) that gaze shifts result from a control principle that optimizes some performance criterion, such as speed-accuracy trade-off, which minimizes the impact of internal noise and uncertainty, or minimization of motor effort.

Fig. 1A illustrates a horizontal sound-evoked gaze saccade, in which the initial eye- and head orientations were aligned at straight ahead. It shows the different stages during and around the gaze shift: (i) the fixation phase, during which the vestibular-ocular reflex (VOR) ensures stable fixation, (ii) the gaze shift ($\Delta G = 26$ degree) consists of a large eye saccade ($\Delta E = 22$ degree) to E_{END}, and a small head-movement contribution ($\Delta H = 4$ degree) with the VOR attenuated. (iii) The gaze shift is followed by a remaining head movement (here 14 degree), during which gaze remains stable because of the VOR. (iv) At the end of the head movement (H_{off}), the eye orientation may be eccentric in the head (here, $E_{\mathrm{off}} = 8$ degree).

Because of the different plant dynamics of eyes and head, and the eye's limited oculomotor range, not all eye-head combinations are possible or equally efficient in reorienting gaze. Typically, small gaze shifts are associated with small head movements, and large gaze shifts with larger head movements, but the latter also depends on initial eye orientation (e.g., Freedman and Sparks, 2000; Goossens and Van Opstal, 1997; Guitton and Volle, 1987; Kardamakis et al., 2010). Thus, when a large head movement contributes to the gaze shift, gaze peak-velocity is reduced. This point is illustrated in Fig. 1B. Because of the much larger head contribution, the gaze velocity of 60 degree gaze shifts tends to be considerably lower than for gaze shifts with an amplitude of 30 degree.

In this report, we propose a quantitative model that explains this behavior. The major novelty of our model with respect to earlier proposals (Daye et al., 2014; Freedman, 2001; Goossens and Van Opstal, 1997; Guitton and Volle, 1987; Kardamakis et al., 2010; Sağlam et al., 2011) resides in the assumed role of the midbrain Superior Colliculus (SC) in the control of gaze shifts. Our model is based on results of recent single-unit recordings, taken from the SC of head-restrained and head-free monkeys, which support the idea that the motor SC acts as the nonlinear vectorial gaze-pulse generator of the system.

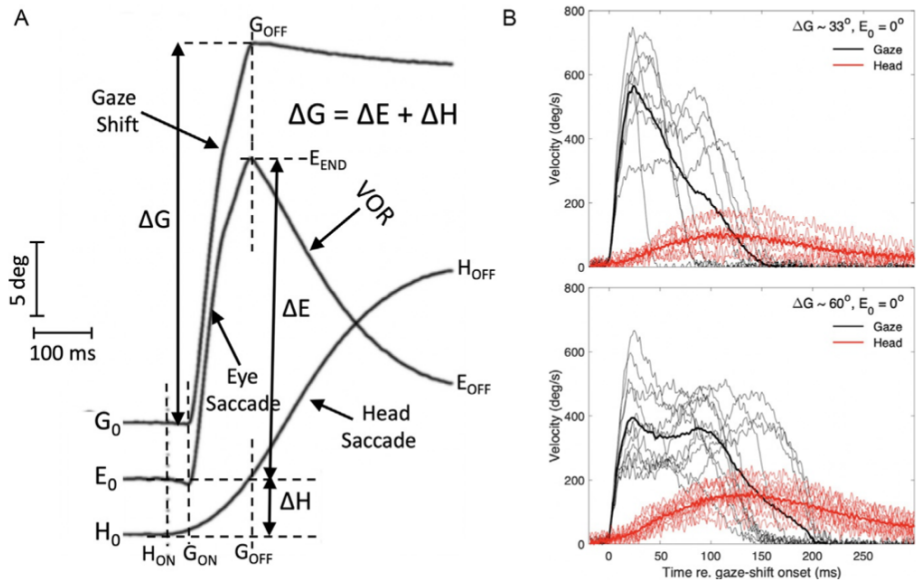

FIG. 1

(A) Example of a horizontal gaze shift (25.5 degree amplitude) to an auditory target with the eyes and head initially aligned (signals are shifted by a few degrees for illustrative reasons). The eye- and head displacements that contribute to the gaze shift are measured between gaze on- and offset (G_{ON}, G_{OFF}; vertical dashed lines). Note that the contribution of the head to the gaze shift ($\Delta H = 3.8$ degree) differs markedly from the overall head displacement (17.6 degree). Note also that the head starts to move slightly earlier than the eyes (H_{ON}), inducing a small vestibular counter movement of the eyes to maintain stable gaze fixation. During the fully operating vestibular ocular reflex (VOR) after gaze offset, gaze remains stable (apart from a slow centripetal drift in darkness), while the head continues to move to its final position, H_{OFF}. (B) Example gaze- (black) and head- (red) velocity profiles for gaze shifts with an amplitude of about 33 degree (top) vs. 60 degree (bottom). In the latter case, the head contribution is considerably larger, causing the overall gaze velocity to drop (see also Fig. 2B). Solid lines: average profiles.

1.2 Brief background SC

The SC contains a topographic map of saccadic gaze shifts (Freedman and Sparks, 1997; Ottes et al., 1986; Robinson, 1972). Prior to and during saccades, a population of cells encodes amplitude and direction by the location of its center within the map (Ottes et al., 1986; Sparks and Mays, 1980). SC recordings in head-restrained monkeys demonstrated that the population also encodes saccade kinematics through their firing rates (Goossens and Van Opstal, 2006).

We thus proposed that the SC issues a desired (straight-line) dynamic eye-displacement signal by its total cumulative number of spikes in the saccade-related bursts. Moreover, all cells in the population synchronize their bursts, such that even

at the single-unit level each cell encodes the straight desired trajectory of any saccade within its movement field (Goossens and Van Opstal, 2012).

We formulated a simple computational model, in which each spike in the burst from each recruited neuron, k, contributes a tiny movement, $\vec{m}_k$, to the saccade. This "spike-vector" is determined by the cell's location in the map, and specifies its connection strength with the brainstem burst generators via the SC-to-brainstem efferent mapping function (Ottes et al., 1986; Van Gisbergen et al., 1987). According to this dynamic ensemble-coding model, the saccade trajectory is encoded by linear cumulative integration of all SC spike vectors:

$$\Delta \vec{E}(t) = \sum_{k=1}^{N_{POP}} \sum_{s=1}^{N_{spk,k}<t} \delta(t-\tau_{k,s}) \cdot \vec{m}_k \qquad (1)$$

where $\delta(t-\tau_{k,s})$ is a spike of cell k, fired at time $t=\tau_{k,s}$.

Simulations with measured spike trains and a *linear* brainstem burst generator demonstrated that the model fully accounted for the nonlinear main-sequence properties and velocity profiles of fast and slow saccades. As a logical consequence, the main-sequence nonlinearity has to reside in the distribution of spike trains and firing rates in the motor SC (Van Opstal and Goossens, 2008).

The hypothesis therefore holds that the SC may embed the neural correlate of the optimal controller underlying gaze shifts (Harris and Wolpert, 1998, 2006). Analysis of single-unit responses revealed that its neural mechanism could be described as follows:

(I) A spatial gradient in the peak-firing rates of SC cells from rostral (small saccades, firing rates up to 900 spks/s) to caudal locations (large saccades, about 300–400 spks/s).
(II) On average, cells fire the *same* number of spikes for their optimal saccade.
(III) The population size is the same (diameter of about 1 mm) for all saccades. Hence, the total number of spikes in each recruited population is the same.
(IV) All cells within the population synchronize their bursts.

We here extend these ideas to the head-unrestrained condition. Monkeys generated eye-head saccades with considerable natural variability in their kinematics, induced by varying the initial eye-in-head position. A critical prediction of Eq. (1) is that the *same* relation should hold for head-unrestrained saccades, regardless gaze-shift kinematics. Thus, the nonlinear gaze kinematics should be reflected in the burst properties of SC cells. To our knowledge, these properties have so far not been documented for head-unrestrained gaze shifts.

2 Methods

Experiments were performed in the laboratory of Dr. EG Freedman at the Department of Neurobiology and Anatomy, School of Medicine and Dentistry of the University of Rochester, NY, while one of the authors (A.J.v.O.) was a visiting

scientist. Two trained rhesus monkeys (P and S) participated in the experiments. Animals were trained to follow briefly flashed visual targets against a small liquid reward by generating rapid eye-head gaze shifts, while single-unit activity from the left SC was recorded. Details on the surgical procedures, training protocols, and experimental setup are described in full detail in Quessy and Freedman (2004), Quessy et al. (2010), and Walton and Freedman (2011). All experimental procedures were approved by the University of Rochester Animal Care and Use Committee, and fully adhered to the National Institutes of Health Guide for the Care and Use of Animals.

We recorded from a total of 52 cells, out of which 30 neurons were isolated long enough for detailed analysis. The movement fields were typically obtained from cells in the caudal SC, where optimal saccade amplitudes ranged from about 30 to 100 degree.

2.1 Paradigm

To vary movement kinematics, monkeys elicited gaze-saccades from different initial eye-in-head orientations. At the start of a trial, the animal looked at a straight-ahead LED while aligning one of three head-fixed lasers with the fixation point. The lasers were positioned such that the horizontal head orientation with respect to straight ahead would be either [−18, 0, +18] degree. For example, a target presented at 60 degree rightward resulted in three different 60 degree eye-head gaze shifts: the head at −18 degree (i.e., the eyes directed 18 degree ipsilateral to the target), 0 degree (eye-head alignment), or +18 degree (the "eye-contra" condition).

2.2 Analysis

To determine the movement field, gaze saccades were elicited in and around the cell's response field. We counted the number of spikes in the burst from 20 ms before gaze-shift onset to 20 ms before offset (e.g., Fig. 3A), and applied the afferent mapping function of Ottes et al. (1986) to each gaze shift to calculate its anatomical coordinates (u,v) in the SC map. In polar coordinates (ΔG, Φ):

$$u = B_u \cdot \ln\left(\frac{\sqrt{\Delta G^2 + 2A \cdot \Delta G \cdot \cos\Phi + A^2}}{A}\right) \text{mm}$$
$$v = B_v \cdot \operatorname{atan}\left(\frac{\Delta G \cdot \sin\Phi}{\Delta G \cdot \cos\Phi + A}\right) \text{mm} \quad (2)$$

where $B_u = 1.4$ mm, $B_v = 1.8$ mm/rad, and $A = 3.0$ degree determine the shape of the monkey afferent mapping function (Ottes et al., 1986; Robinson, 1972; Fig. 4).

We first fitted the *static movement field* function to all gaze-saccade vectors, and included a potential eye-in-head gain-field modulation (Van Opstal et al., 1995) by the initial eye position, E_0, to the total number of spikes in the burst, N, according to:

$$N(\Delta G, \Phi, E_0) = N_0 \cdot (1 + \varepsilon \cdot E_0) \cdot \exp\left(-\frac{(u-u_0)^2 + (v-v_0)^2}{2\sigma_P^2}\right) \quad (3)$$

This model has five free parameters: N_0 is the number of spikes in the burst for the optimal saccade from straight ahead, (u_0,v_0) (in mm) are the SC coordinates of the optimal saccade (Eq. 2), ε (in #spikes/degree) is the eye-position gain, and σ_P (in mm) quantifies the tuning width. Optimal parameter values were obtained with the Nelder–Mead Simplex algorithm in MATLAB®.

Next, the *dynamic* movement field describes how the cumulative number of spikes in the burst evolves during the straight gaze-displacement along the line connecting start- and end-positions (Goossens and Van Opstal, 2006). According to this model, the cumulative spike count for any gaze shift, regardless its kinematics, obeys the following, linear, relation:

$$CS(\Delta G, \Phi, E_0, t) = \Delta G(t+\tau) \cdot \frac{N(\Delta G, \Phi, E_0)}{\Delta G} \quad (4)$$

where $\Delta G(t+\tau)$ is the desired straight trajectory (increasing monotonically from 0 to ΔG). The neuron's lead time, τ, was fixed at $\tau = 20$ ms for all neurons. The straight trajectory was obtained by projecting the actual trajectory $(x(t), y(t))$ onto gaze vector $\Delta G \cdot (\cos\Phi, \sin\Phi)$ (Goossens and Van Opstal, 2006):

$$\Delta G(t) = x(t) \cdot \cos\Phi + y(t) \cdot \sin\Phi \quad (5)$$

The time-independent factor in Eq. (4), $N(\Delta G, \Phi, E_0)/\Delta G$, corresponds to the slope of the dynamic phase-relation. It should vary in a systematic way with gaze-shift amplitude and direction (Goossens and Van Opstal, 2006).

3 Results

3.1 Behavior

Fig. 2 shows an analysis of representative gaze shifts from monkey S for the three initial eye positions. These mainly horizontal gaze shifts (amplitudes between 20 and 75 degree) were directed into the movement field of neuron s1809. The contribution of the head movement to the gaze shift (see Fig. 1, for definition) depended systematically on the gaze-shift amplitude and initial eye-position (Fig. 2A), and had a strong influence on the peak gaze-velocity (Fig. 2B), and gaze-saccade duration (Fig. 2C). Note that for the largest gaze shifts, peak gaze velocity even tended to decrease with gaze-shift amplitude, which was highly significant for the contra- ($r = -0.46$) and centered ($r = -0.63$) eye positions. This property is due to two factors: first, for increasing gaze amplitudes the contribution of the (slower) head movement increases (Figs. 1B and 2A). Second, for large gaze shifts, the eyes will

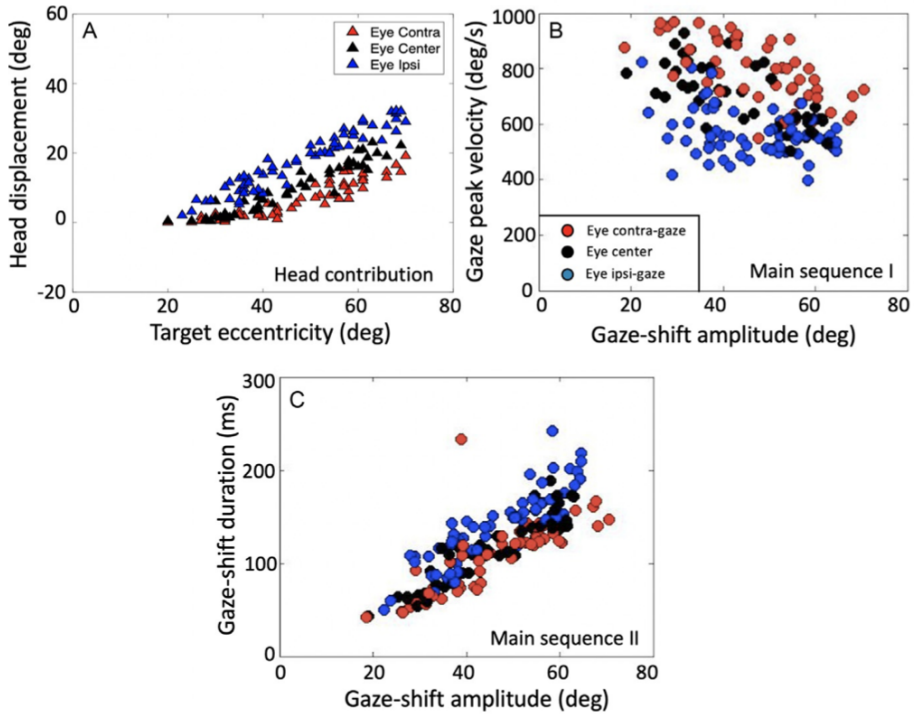

FIG. 2

Properties of monkey eye-head gaze shifts, measured during single-unit recording of neuron s1809 (see Fig. 3). Rightward gaze shifts ($N = 180$) up to 75 degree amplitude were elicited into the cell's movement field, for three initial eye-in-head orientations (colors). (A) The contribution of the head movement varied systematically with initial eye position. (B,C) The initial fixation conditions had a strong influence on the gaze kinematics: larger/smaller head movements yielded slower/faster gaze shifts. Peak gaze velocities thus varied by >40%. Note also the significant decline of peak gaze velocity for the larger gaze shifts for the contralateral (red) and central (black) initial eye positions.

approach their oculomotor range so that the eye-in-head velocity starts to plateau. As a result, the later (slower) part of the head movement will increasingly dominate the gaze velocity. Ipsilateral eye orientations (blue symbols) caused consistently larger head movements, and the slowest gaze shifts. The fastest gaze shifts were obtained for contralateral initial eye orientations. These findings were robust for all recording sessions and for both monkeys.

3.2 Neural responses

The changes in initial eye-position also affected the activity of SC neurons. This is documented in Fig. 3 for neuron s1809. Fig. 3A shows the raw spike trains for the gaze shifts of Fig. 2. The neuron fires a prominent saccade-related burst associated with the upcoming saccade. Fig. 3B presents the phase plots for these spike trains.

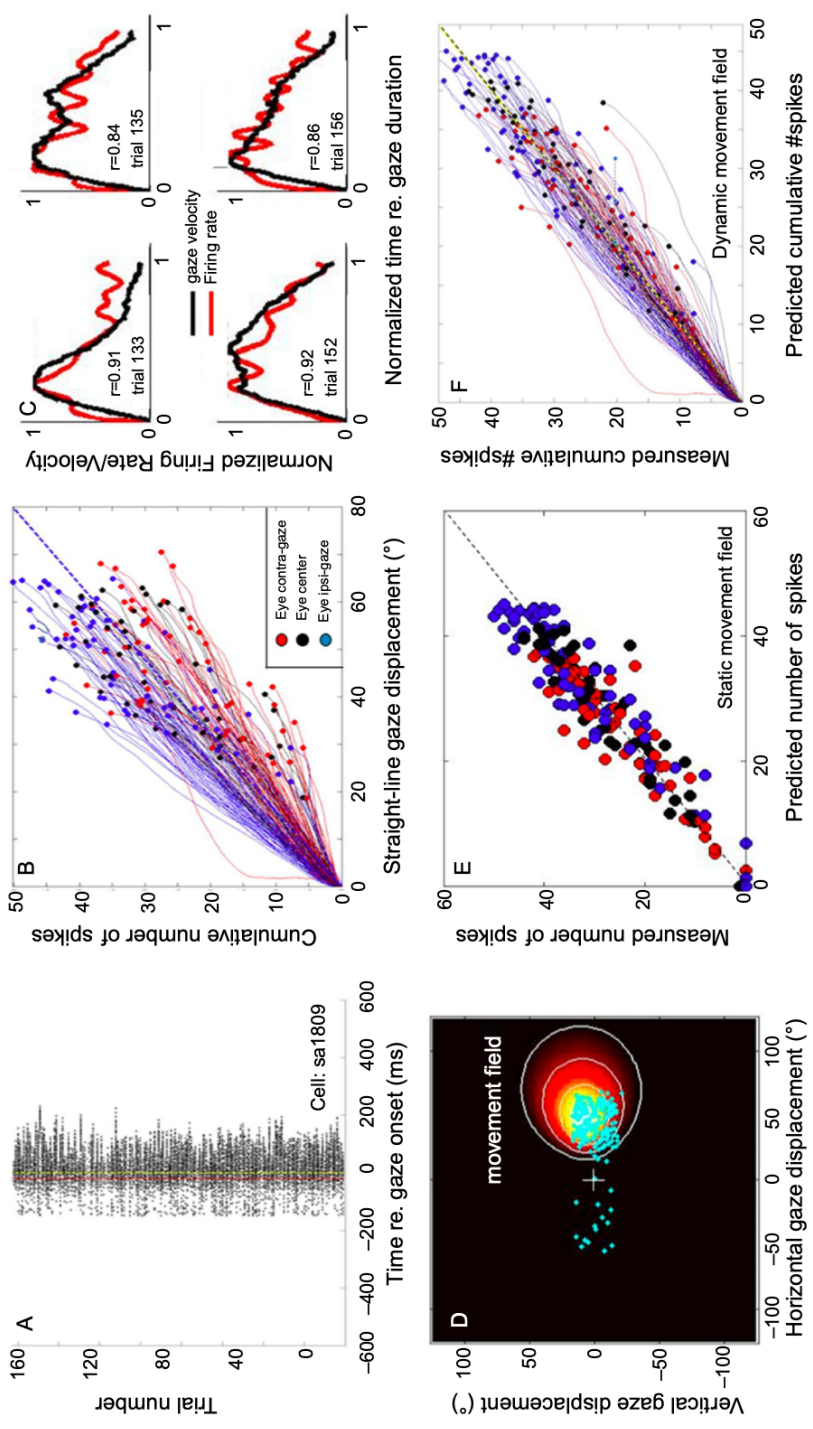

FIG. 3

(A) Raw spike trains of cell s1809 for all 180 trials into its movement field, aligned to gaze-movement onset (yellow-dashed line at $t = 0$). The motor burst starts 20 ms before gaze onset (red-dashed line). (B) Phase trajectories of the cumulative number of spikes as function of ongoing gaze displacement along the straight gaze vector. (C) Four example trials demonstrating a tight correlation between the cell's firing-rate profile and instantaneous gaze velocity. For ease of comparison, both variables were normalized to gaze duration and to their maxima. (D) Plot of the movement field (Eq. 3) in gaze-vector coordinates; color specifies number of spikes (dark: low, light: high). Cyan dots: endpoints of the gaze-shift vectors elicited during the neural recording. (E) The gain-field model captures the data well for all gaze shifts and initial conditions. (F) Test of Eq. (4) on the spike trains during all fast (red), intermediate (black), and slow (blue) gaze shifts into the movement field.

It shows the cumulative number of spikes, $CS(t+20)$, as function of the dynamic gaze-shift vector, $\Delta G(t)$. Note that each phase trajectory follows an approximately straight line, for which slope and end point differed considerably for each trial. According to Eq. (4), this slope should depend on the total number of spikes in the burst (as determined by Eq. 3), and gaze-saccade amplitude. It is immediately clear that the cumulative number of spikes in the burst also depends on initial eye position, as blue, black and red phase trajectories fall into different clusters. To test whether the dynamic movement-field model of Eq. (4) captures this variability in the cell's spiking behavior, we first determined the static movement field of the cell by fitting Eq. (3) to the total spike counts. Fig. 3D shows the movement field of the cell, together with all 180 gaze-saccade endpoints (cyan dots) for this experiment. The optimal parameters for this neuron were:

$N_0 = 40.3$ spikes	$\Delta G_0 = 57.2$ degree	$\Phi_0 = 9.4$ degree	$u_0 =$ 4.2 mm	$v_0 =$ 0.28 mm	$\sigma_P =$ 0.73 mm	$\varepsilon = 0.0063$ spikes/ degree

In Fig. 3E we show that the total number of spikes in the burst is predicted well by this model ($r = 0.96$). Fitting the movement field without eye-position modulation yielded $r = 0.90$, which is significantly lower ($P < 0.0001$). We next determined the predictions for the slopes of the spike-train phase trajectories of Fig. 3B (Eq. 4). Fig. 3F shows the predicted cumulative number of spikes for each response vs. the measured cumulative spike count. Note that this plot contains >20,000 data points. Yet, the correlation between measurements and predictions is very high: $r = 0.96$.

We observed that the neuron's firing rate had a remarkably good resemblance with instantaneous gaze velocity along the desired trajectory for a large fraction of trials. To illustrate this point, Fig. 3C shows four example trials with different gaze-velocity profiles. These normalized traces appeared to correlate very well. We obtained correlations $r > 0.7$ for nearly 50% of the trials in the majority of cells (results to be published elsewhere; see Section 4).

3.3 Model

Based on the behavioral and neurophysiological results we propose a computational model for the generation of eye-head gaze shifts, in which the SC provides the common drive for the eyes and head as a dynamic desired straight gaze trajectory, $\Delta G(t)$, by its total cumulative number of spikes. In other words, the instantaneous firing rate of the total population specifies the desired gaze velocity profile, and as such acts as a *vectorial gaze-pulse generator*. Details of the model, which is presented in its conceptual form in Fig. 4, including simulations, were published recently in Kasap and Van Opstal (2018a).

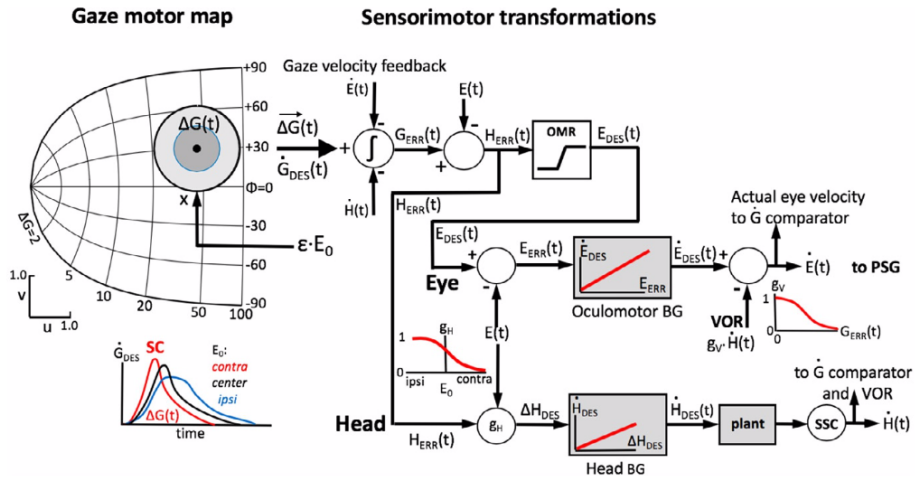

FIG. 4

Computational scheme for dynamic ensemble-coding of saccadic eye-head gaze shifts by the collicular population. The desired gaze-velocity profile along the straight trajectory, $\Delta G(t)$, is issued by the SC population, on which the initial eye position, E_0, exerts a weak, multiplicative modulation. Thus, in line with our recordings, the number of spikes in the burst, and the spike timings, depends on eye position too (e.g., Fig. 3C and E). Eye and head are driven by different signals in head-centered reference frames. The actual contributions of the eye and head movements to the gaze shift, ΔE, and ΔH, depend on E_0 through gain g_H (inset) and on their relative timings. The VOR gain is modulated between 0 and 1 by ongoing gaze error, $G_{ERR}(t)$ (inset). PSG: pulse-step generator and oculomotor plant (not shown). The relative onsets of eye- and head movements depend on stimulus modality, initial eye position, and top-down task-related signals (not shown).

The SC output represents the desired straight-line gaze velocity, $\dot{G}_{DES}(t)$, which is compared with the true gaze velocity from the oculomotor and head-motor systems to determine a dynamic gaze-error signal:

$$G_{ERR}(t) = \int_{ON}^{t} \left(\dot{G}_{DES}(\tau) - \dot{E}(\tau) - \dot{H}(\tau)\right) d\tau \tag{6}$$

This gaze error is combined with eye position to represent the dynamic error of the gaze saccade in a *craniocentric* reference frame:

$$H_{ERR}(t) = G_{ERR}(t) + E(t) \tag{7}$$

This latter signal drives both the oculomotor and head-motor systems. For the eye, the signal can keep eye position within the (soft) oculomotor range (OMR). The dynamic desired eye-in-head position thus becomes:

$$E_{DES}(t) = OMR\left(H_{ERR}(t)\right) \tag{8}$$

This signal drives the (linear) oculomotor burst generator with dynamic eye motor-error:

$$E_{ERR}(t) = E_{DES}(t) - E(t) \tag{9}$$

The output of the oculomotor burst generator represents *desired* eye velocity:

$$\dot{E}_{DES}(t) = B_E \cdot E_{ERR}(t) \tag{10}$$

with B_E (in s^{-1}) a linear gain. Finally, the actual eye velocity during eye-head gaze shifts is obtained after combining this signal with the VOR:

$$\dot{E}(t) = \dot{E}_{DES}(t) - g_V(G_{ERR}(t)) \cdot \dot{H}(t) \tag{11}$$

where the VOR gain ($0 < g_V < 1$) is a nonlinear sigmoid function of instantaneous gaze error: it is close to one (fully engaged) when the gaze error is small, and approaches zero (it is off) for large gaze errors (inset in Fig. 4).

In our model also the head is driven by the dynamic head-motor error (see inset in Fig. 4):

$$\Delta H_{DES}(t) = g_H(E_0) \cdot H_{ERR}(t) \tag{12}$$

where the gain $0 < g_H < 1$ is a nonlinear function of initial eye position. The desired head velocity is subsequently generated by a linear head-burst generator:

$$\dot{H}_{DES}(t) = B_H \cdot \Delta H_{DES}(t) \tag{13}$$

where $B_H < B_E$. The actual head velocity results after passing the desired motor drive through the head-motor plant:

$$\dot{H}(t) = PLANT_{HEAD}\left(\dot{H}_{DES}(t)\right) \tag{14}$$

for which we took a simple first-order low-pass filter. Simulations with this model show that it faithfully captures the kinematics and eye-head cross-coupling properties of measured eye-head gaze shifts (Kasap and Van Opstal, 2018a).

4 Discussion

We extended our SC model of dynamic movement fields (Goossens and Van Opstal, 2006) by including a small, but significant, influence of initial eye-in-head position on the total number of spikes in the burst (gain-field model, Eq. 3). We noted that eye position systematically influenced the SC firing-rate profiles:

Ipsilateral eye	Lower firing rates	Longer burst durations	More spikes
Contralateral eye	Higher firing rates	Shorter burst durations	Fewer spikes

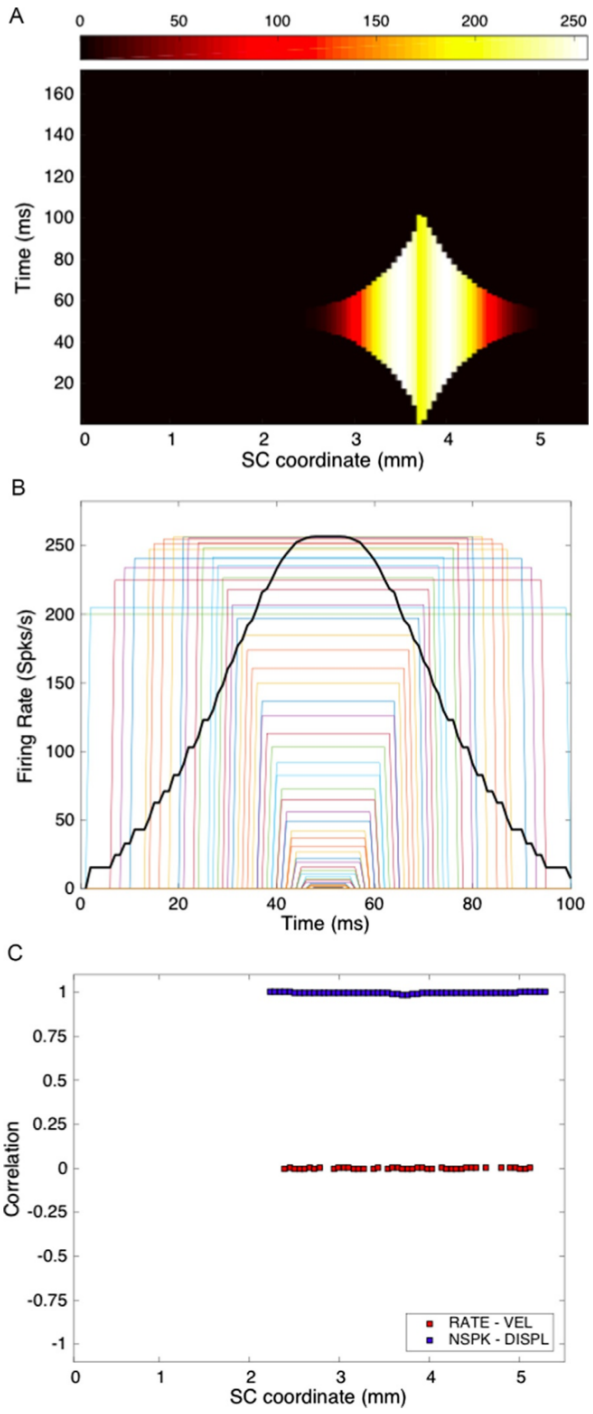

FIG. 5

See legend on opposite page.

In many trials (~50%) we found a tight correlation ($r > 0.7$) between the instantaneous firing rate of an SC cell and the straight-line gaze-velocity profile into their movement fields (e.g., Fig. 3C). An eye-position signal in the motor SC has been reported before (Van Opstal et al., 1995), but its potential role for the control of gaze kinematics in eye-head saccades has not been reported.

Note that the linear spike-counting model (Eq. 1) is a *population model*. As such, it predicts that the *total* collicular output faithfully reflects the instantaneous desired gaze displacement (cumulative spike count) and gaze velocity (total cumulative firing rate). The model does *not* necessarily predict that individual cells should reflect gaze kinematics on a trial-by-trial basis.

To illustrate this point, Fig. 5 shows a simulation with rectangular SC bursts (Fig. 5B), with the number of spikes determined by the static movement field. The total SC output still produced the required gaze-velocity (Fig. 5B) and gaze trajectory, even though none of the cells encode gaze velocity ($r = 0$; Fig. 5C). Therefore, the tight correlation illustrated in Fig. 3C underscores the role for the motor SC as the nonlinear vectorial pulse generator of the saccadic gaze-controller, as proposed in our model (Fig. 4).

In head-restrained monkeys, we found that spike trains correlated well with instantaneous eye-velocity because of the tight synchronization of burst profiles across the population (Goossens and Van Opstal, 2012). We recently reported that this important aspect of neural population activity can be understood from excitatory-inhibitory lateral interactions among the SC cells in a spiking neural network (Kasap and Van Opstal, 2017, 2018b; Van Opstal and Kasap, 2018).

We here conjecture that a similar control principle may hold for eye-head gaze saccades, whereby initial eye position influences the characteristics of SC cells in such a way that (i) their burst characteristics vary with initial eye orientation, and (ii) the total number of spikes changes too.

In our spiking neural network model (Kasap and Van Opstal, 2017, 2018b; Van Opstal and Kasap, 2018), the burst characteristics of spiking leaky-integrate-and-fire neurons depended on two parameters: the time constant of the membrane adaptation current, and the scaling strength of the synaptic weights that make up the lateral

FIG. 5

Simulation of a hypothetical SC–brainstem saccade model (one-dimensional, for clarity), in which all cells fire rectangular bursts. (A) Population activity in the SC motor map as function of time for a gaze shift of 30 degree. Color code represents mean firing rates. Cells at the fringes of the population start their shorter bursts later than the central cells, so that all cells reach their peak at the same time. (B) Rectangular bursts of all cells; the number of spikes of each cell is determined by the static movement field; burst duration decays exponentially with distance from the central hot spot at $u = 3.7$ mm. Continuous curve: instantaneous (normalized) firing rate (representing gaze velocity) of the population. (C) The cumulative number of spikes for each individual cell correlates well with instantaneous gaze displacement (blue), but firing rates of individual cells do not correlate at all with instantaneous gaze velocity (red).

excitatory-inhibitory interactions. To ensure a fixed number of spikes in the central burst of the population, and a systematic decrease of peak firing-rate with saccade amplitude, both parameters had to depend systematically on the cell's rostral-caudal location in the motor map. We here speculate that initial eye position may affect the values of these parameters for the upcoming gaze shift, leading to the observed modifications of the burst characteristics and ensuing gaze kinematics.

As a result of eye-head coupling, the inclusion of the VOR, the oculomotor range, and the eye-position influence on SC cells, each of which introduces its own nonlinearity in the system, the computational complexity of the model is markedly increased when compared to the simple linear eye-movement model of Goossens and Van Opstal (2006). Moreover, the variable onsets of eye- and head-movements in the gaze shift, and thus their contribution and kinematics, depend on various factors, such as initial eye position, stimulus modality, and task constraints. Thus, at first sight, one would not immediately expect that firing rates of SC neurons would correlate so well with the dynamic gaze trajectory.

As a final note, our model concentrated mainly on the role of the SC in gaze control, and less on the question whether downstream brainstem-cerebellar-spinal circuitry operates with a gaze feedback loop (like Fig. 4, and in the models of Goossens and Van Opstal, 1997; Guitton and Volle, 1987; Kasap and Van Opstal, 2018a; Sağlam et al., 2011), or without gaze-feedback by controlling independent, but coupled eye-head circuits (like in the models of Daye et al., 2014; Freedman, 2001; Kardamakis et al., 2010). We believe that our collicular data do not rule out either hypothesis, as the SC responses already seem to reflect all major properties of the ensuing gaze shifts and their kinematics.

Acknowledgments

This work was supported by EU Horizon 2020 ERC Advanced Grant ORIENT (nr. 693400, A.J.v.O., B.K.) and by the Radboud University (A.J.v.O.). The authors are highly indebted to Ed Freedman, Mark Walton, and Stephan Quessy from the Department of Neuroscience at the University of Rochester, NY, USA, for hosting A.J.v.O. in their lab (May–June 2009), to share their excellent facilities, their time and expertise that enabled the experiments, and for many fruitful discussions.

References

Daye, P.M., Optican, L.M., Blohm, G., Lefèvre, P., 2014. Hierarchical control of two-dimensional gaze saccades. J. Comput. Neurosci. 36, 355–382.

Freedman, E.G., 2001. Interactions between eye and head control signals can account for movement kinematics. Biol. Cybern. 84, 453–462.

Freedman, E.G., Sparks, D.L., 1997. Eye-head coordination during head-unrestrained gaze shifts in rhesus monkeys. J. Neurophysiol. 77, 2328–2348.

Freedman, E.G., Sparks, D.L., 2000. Coordination of the eyes and head: movement kinematics. Exp. Brain Res. 131, 22–32.

Goossens, H.H.L.M., Van Opstal, A.J., 1997. Human eye-head coordination in two dimensions under different sensorimotor conditions. Exp. Brain Res. 114, 542–560.
Goossens, H.H.L.M., Van Opstal, A.J., 2006. Dynamic ensemble-coding of saccades in the monkey superior colliculus. J. Neurophysiol. 95, 2326–2341.
Goossens, H.H.L.M., Van Opstal, A.J., 2012. Optimal control of saccades by spatial-temporal activity patterns in monkey superior colliculus. PLoS Comput. Biol. 8 (5), e1002508.
Guitton, D., Volle, M., 1987. Gaze control in humans: eye-head coordination during orienting movements to targets within and beyond the oculomotor range. J. Neurophysiol. 58, 427–459.
Harris, C.M., Wolpert, D.M., 1998. Signal-dependent noise determines motor planning. Nature 394, 780–784.
Harris, C.M., Wolpert, D.M., 2006. The main sequence of saccades optimizes speed-accuracy trade-off. Biol. Cybern. 95, 21–29.
Kardamakis, A.A., Moschovakis, A.K., 2009. Optimal control of gaze shifts. J. Neurosci. 29, 7723–7730.
Kardamakis, A.A., Grantyn, A., Moschovakis, A.K., 2010. Neural network simulations of the primate oculomotor system. V. Eye–head gaze shifts. Biol. Cybern. 102, 209–225.
Kasap, B., Van Opstal, A.J., 2017. A spiking neural network model of the midbrain superior colliculus that generates saccadic motor commands. Biol. Cybern. 111, 249–268.
Kasap, B., Van Opstal, A.J., 2018a. Double stimulation in a spiking neural network model of the midbrain superior colliculus. Front. Appl. Math. Stat. 4, 47. https://doi.org/10.3389/fams.2018.0047.
Kasap, B., Van Opstal, A.J., 2018b. A model for auditory-visual evoked eye-head gaze shifts in dynamic multi-steps. J. Neurophysiol. 119, 1796–1808.
Ottes, F.P., Van Gisbergen, J.A.M., Eggermont, J.J., 1986. Visuomotor fields of the superior colliculus: a quantitative model. Vision Res. 12, 1795–1808.
Quessy, S., Freedman, E.G., 2004. Electrical stimulation of rhesus monkey nucleus reticularis gigantocellularis. I. Characteristics of evoked head movements. Exp. Brain Res. 156, 342–356.
Quessy, S., Quinet, J., Freedman, E.G., 2010. The locus of motor activity in the superior colliculus of the rhesus monkey is unaltered during saccadic adaptation. J. Neurosci. 30, 14235–14244.
Robinson, D.A., 1972. Eye movements evoked by collicular stimulation in the alert monkey. Vision Res. 12, 1795–1808.
Sağlam, M., Lehnen, N., Glasauer, S., 2011. Optimal control of natural eye-head movements minimizes the impact of noise. J. Neurosci. 31, 16185–16193.
Sparks, D.L., Mays, L.E., 1980. Movement fields of saccade-related burst neurons in the monkey superior colliculus. Exp. Brain Res. 190, 39–50.
Van Gisbergen, J.A.M., Van Opstal, A.J., Tax, A.A.M., 1987. Collicular ensemble coding of saccades based on vector summation. Neuroscience 21, 541–555.
Van Opstal, A.J., Goossens, H.H.L.M., 2008. Linear ensemble coding in midbrain superior colliculus specifies the saccade kinematics. Biol. Cybern. 98, 561–577.
Van Opstal, A.J., Kasap, B., 2018. Electrical stimulation in a spiking neural network model of monkey superior colliculus. In: Mathematical Modeling in Motor Neuroscience: State of the Art and Translation to the Clinic. Progress in Brain Research, vol. 248. Elsevier.
Van Opstal, A.J., Hepp, K., Suzuki, Y., Henn, V., 1995. Influence of eye position on activity in monkey superior colliculus. J. Neurophysiol. 74, 1593–1610.
Walton, M.M.G., Freedman, E.G., 2011. Gaze-shift duration, independent of amplitude, influences the number of spikes in the burst for medium-lead burst neurons in pontine reticular formation. Exp. Brain Res. 214, 225–239.